Title

A 2D percolation-based model for characterizing the piezoresistivity of carbon nanotube-based films

Journal

Journal of Materials Science, 50(7)

ISSN

0022-2461

Authors

Lee, Bo Mi

Loh, Kenneth J

Publication Date

2015-04-01

DOI

10.1007/s10853-015-8862-y

Peer reviewed

A 2D percolation-based model for characterizing the piezoresistivity of carbon nanotube-based films

Bo Mi Lee

Kenneth J. Loh*

Department of Civil & Environmental Engineering, University of California, Davis, CA 95616, USA.

Phone: +1 530-754-9428

Fax: +1 530-752-7872

*Corresponding Email: kjloh@ucdavis.edu

Webpage: http://nesst.engr.ucdavis.edu

Abstract

Carbon nanotubes (CNT) have attracted considerable attention due to their unique electrical, mechanical, and electromechanical properties. In particular, thin films formed by embedding CNTs in polymer matrices have been shown to exhibit strain-sensitive electromechanical properties, which can serve as an alternative to traditional strain sensors. Although numerous experimental studies have characterized their electrical properties and piezoresistivity, it remains unclear as to what nano-scale mechanisms dominate to govern nanocomposite electromechanical properties. Therefore, the objective of this study is to create a two-dimensional (2D) percolation-based numerical model to understand the electrical and coupled electromechanical behavior of CNT-based thin films. First, a percolation-based model with randomly dispersed straight nanotubes was generated. Second, the percolation and unstrained electrical properties of the model were evaluated as a function of CNT density and length. Next, uniaxial tensile-compressive strains were applied to the model for characterizing their electromechanical response and piezoresistivity. In addition, the effects of different intrinsic strain sensitivities of individual nanotubes were also considered. The results showed that bulk film strain sensitivity was strongly related to CNT density, length, and its intrinsic strain sensitivity. In particular, it was found that strain sensitivity decreased with increasing CNT density. While these strain sensitivity trends were consistent for different intrinsic CNT gage factors, the results were more complicated near the percolation threshold. These results were also compared to other experimental research

so as to understand how different nano-scale parameters propagate and affect bulk film response.

Keywords: *carbon nanotube; electromechanical properties; numerical model; percolation; piezoresistivity; strain sensing; thin film.*

Introduction

Carbon nanotubes (CNT) are long and hollow cylindrically shaped nanomaterials that physically represent that of a rolled graphene structure. They can exist as single-walled (SWNT) or multi-walled carbon nanotubes (MWNT), which depends on the number of concentrically stacked tubes. While MWNTs are metallic, SWNTs can be semiconducting or metallic depending on its chirality. Their popularity for engineering applications ([1-5]) is largely due to their impressive intrinsic properties [3], which are derived from their unique nano-scale structure [3,4,6]. To be specific, CNTs are characterized by extremely high aspect ratios, where its diameter can be as small as 0.4 nm, while its length can be up to a few centimeters [4,6]. In addition, the surface of nanotubes, like each layer of graphite or graphene, consists of strong carbon-carbon covalent bonds [6]. This interesting structure results in exceptional mechanical properties; for instance, the Young's modulus and bending strength of MWNTs can be up to 1.28 TPa and 63 GPa, respectively [1]. In addition, its one-dimensional (1D)-like structure enables each nanotube to transport electrons almost without scattering, which results in near-ballistic electron transport properties [3,7]. In fact, the electrical conductivity of SWNTs and MWNTs have been found to be up to 10^6 and 10^5 S-cm^{-1}, respectively [8].

However, as with many nanomaterials, carbon nanotubes also tend to agglomerate in its pristine form, and it becomes challenging to take advantage of their unique properties in this case [9]. Scalability is another issue in which some applications demand the fabrication of tangible devices that incorporate nanomaterials such as CNTs [10]. To overcome these two challenges, one solution is to create nanocomposites by embedding dispersed nanotubes within a polymer matrix [11]. In doing so, the polymer matrix can prevent CNTs from re-agglomerating (as they would in many

solutions or solvents), while the nanocomposite becomes easier to handle, manipulate, and use. As an example, researchers have investigated CNT-polymer nanocomposites for fabricating next-generation ultra-strong coatings [12]. Specifically, when nanotubes are embedded in the polymer matrix, the nanocomposite's mechanical properties (*e.g.,* stiffness and strength) can be significantly enhanced. Gojny *et al.* [13] demonstrated that the stiffness and fracture toughness of 1 wt% CNT-epoxy composites increased by 6% and 26%, respectively. Similarly, Qian *et al.* [14] showed that the stiffness of 1 wt% CNT-polystyrene composites improved by ~40% compared to that of the pristine polymer.

Besides using CNTs for mechanical reinforcement, one can also take advantage of their high electrical conductivity for fabricating thin film strain sensors. Early research by Dharap *et al. [15]* and Li *et al.* [16] proposed buckypaper-type strain sensors fabricated by mixing unpurified SWNTs with *N,N*-dimethylformamide, filtering the solution, and then peeling off the thin film after drying. The buckypaper showed linear changes in electrical properties (*i.e.*, current-voltage response) when subjected to mechanical deformations (*i.e.*, exhibiting piezoresistivity). Kang *et al. [17]* also employed buckypaper and proposed them for detecting strain and cracks. On the other hand, Loh *et al.* [18] employed a layer-by-layer method for assembling mechanically strong SWNT-polyelectrolyte (PE) thin films that were also multifunctional. The nanocomposite was designed for strain or corrosion/pH, and its functionality depended on the specific polymer or PE incorporated during film fabrication. Continued research also showed that the strain sensitivities of the SWNT-PE thin films could be tuned by controlling the concentration of nanotubes and PE [19]. Other related studies include one by Pham *et al. [20]*, in which they employed two different fabrication methods (*i.e.*, dry-blended and solution-based) and compared the resulting films' electromechanical response. Park *et al*. [21] showed that when deformations were applied to MWNT-polymer films, its electrical resistance increased

linearly up to a maximum threshold of strain before becoming nonlinear, as was also shown by Loyola *et al*. [22].

Complementing experimental research on CNT-based nanocomposites are numerical studies that focused on advancing the fundamental understanding of these materials and the underlying mechanisms that enabled piezoresistivity. To be specific, the inherent properties of individual CNTs (*e.g.*, intrinsic piezoresistivity, diameter, and length, among others) and how they are incorporated in the nanocomposite (*e.g.*, CNT density) can affect the bulk film's electrical, mechanical, and coupled electromechanical properties. In particular, a significant amount of research was dedicated to understanding the nominal electrical properties of CNT-based thin films. As an example, Kumar *et al.* [23] estimated the conductance of a nanotube network model and considered parameters including channel length between source and drain electrodes and nanotube density. Behnam *et al.* [24] investigated how different parameters (*e.g.,* alignment, resistance ratio, nanotube length, and nanotube density) affected the resistivity of a three-dimensional (3D) model created by stacking multiple two-dimensional (2D) nanotube layers. Li *et al. [25]* conducted Monte Carlo simulations and demonstrated that wavy nanotube networks had lower conductivity than that which included only straight nanotubes. In addition, Du *et al.* [26] and Bao *et al.* [27] investigated alignment effects on the electrical properties of 2D and 3D model, respectively.

Building on the body of work dedicated to understanding the electrical properties of CNT-based nanocomposites, many researchers also utilized these thin film numerical models to investigate their electromechanical or strain sensing response. For example, Hu *et al.* [28] regarded tunneling effect as the core parameter that affected the piezoresistive response of CNT-polymer nanocomposites, and the model incorporated an approximate tunneling resistance between neighboring nanotubes. The findings were that

higher sensitivity could be achieved when the density of CNTs was near the percolation threshold. Continued research explored the numerical modeling of tensile and compressive loading, and the results demonstrated that strain sensitivity was higher in tension than compression [29]. Rahman *et al. [30]* also regarded tunneling phenomenon as the dominant parameter that governed bulk film piezoresistivity, and the numerical model considered how tunneling resistance affected strain sensitivity. Amini *et al. [31]* investigated how CNT densities and model dimensions affected the model's electromechanical response, as well as simulation repeatability. Wang *et al. [32]* suggested that the piezoresistivity of CNT-polymer composites could be optimized by maximizing the value of average junction gap variation (AJGV), which consisted of parameters including Poisson's ratio of the polymer and the diameter, orientation, and density of carbon nanotubes.

Despite these advances, additional research on CNT-based thin film numerical modeling is needed for complementing and explaining results obtained from experimental investigations. For instance, thin film piezoresistivity was shown to vary depending on the method and types of polymers and nanotubes employed during fabrication. To be specific, different trends of strain sensitivities as a function of nanotube concentrations were investigated with different fabrication methods [18,29]. Furthermore, the intrinsic piezoresistivity of individual nanotubes and incorporating this parameter as part of bulk nanotube network models have not been emphasized, even though each nanotube could be regarded as a nano-scale strain sensor [7]. In fact, Stampfer *et al. [33]* showed that the gage factor (or strain sensitivity) of an SWNT could be as high as 2,900. Cullinan *et al.* [34] considered a resistor network with 100 nanotubes and demonstrated that the gage factor of the model was 78.5.

In this study, the objective was to implement a 2D percolation-based computational model for investigating the piezoresistive response of CNT-

based nanocomposites. In addition to characterizing the effects of nanotube parameters (*e.g.*, length and density) on thin film nominal electrical properties, this work also focused on incorporating the effects of the inherent piezoresistivity of individual nanotubes. Three different CNT gage factors were considered, which were based on results reported in the literature. Uniaxial tensile-compressive cyclic loads were applied to the nanocomposite model, and its electromechanical properties (such as bulk film strain sensitivity) were calculated and compared. This paper begins with a discussion of the percolation-based model, assumptions, and boundary conditions. Second, the method used for calculating thin film resistance is presented. Then, the results are discussed, followed by a brief summary and future research directions.

Background on Modeling and Simulation

Percolation-based Model

Percolation theory was introduced by Broadbent and Hammersley [35,36] in 1957 to explain phase transition of a permeable 3D box. They demonstrated that low concentrations of fluid could not flow through the permeable box until the fluid concentration reached a certain percolation threshold. Later in 1973, Kirkpatrick [37] applied percolation theory to describe, through numerical modeling, phase transition (*i.e.*, insulator-to-conductor) of conductive particle-based composites.

Similar to these early investigations, one can also expect the same insulator-to-conductor phase transition with the incorporation of electrically conductive nanotubes embedded in an insulating polymer matrix. In particular, three different states can be investigated depending on the concentration of nanotubes. The first state corresponds to when that of the insulating polymer matrix is dominating the electrical properties of the

nanocomposite (Fig. 1). Since very few conductive nanotubes are embedded in the polymer matrix, a continuous conductive pathway for electrical current to flow from one end of the nanocomposite to the other does not exist. As the concentration of nanotubes increases, they start to create electrically conductive clusters, which are formed by direct nanotube-to-nanotube junctions or other electron transport mechanisms between neighboring CNTs (*e.g.*, tunneling). At the second state, with the addition of more nanotubes, the clusters are finally able to connect and form an electrically conductive path between the two opposite electrodes (Fig. 1). After the formation of one conductive pathway, any additional nanotubes will induce dramatic increases in conductivity of the nanocomposite (*i.e.*, due to more routes for current flow). The minimum concentration of nanotubes that causes a remarkable increase in bulk film electrical conductivity (*i.e.*, the transition from an insulator to conductor) is defined as the percolation threshold. The final state corresponds to the case with high CNT concentrations (Fig. 1). Here, a dense network of electrical conductive paths exists, and electrical conductivity increases gradually and finally saturates.

Modeling and Simulation Procedures

To investigate the electrical and electromechanical properties of CNT-based nanocomposites, a 2D percolation-based model was derived by randomly distributing straight 1D nanotubes of a predefined length (L_{CNT}). The concentration of nanotubes (N) and the dimensions of the 2D thin film model (*i.e.*, length, L and width, W) were specified. It should be mentioned that a 2D model was employed for reducing computational demand and as a preliminary effort prior to the implementation of a 3D model (which is the focus of future studies). The location of each nanotube was identified by two end-points, namely (x_1, y_1) and (x_2, y_2), as represented in a Cartesian coordinate system. The first end-point, (x_1, y_1), was determined using a random number generator (*e.g.*, “rand” in *MATLAB*). The other end point, (x_2,

y_2), was then calculated using the prescribed nanotube length and a randomly generated CNT orientation (θ):

$$x_2 = x_1 + L_{CNT}\cos\theta \quad (1)$$

$$y_2 = y_1 + L_{CNT}\sin\theta \quad (2)$$

This procedure was reiterated until the exact number of nanotubes desired (N) was included in the model. A representative numerical model with 400 CNTs in a 1×1 μm^2 area is shown in Fig. 2.

In a previous study, if a portion of the nanotube exceeded the boundary of the thin film model, that portion of the CNT was eliminated so that all the nanotubes fit inside the modeling domain [38]. In contrast, this study employed periodic boundary conditions (PBC) commonly used in creating representative volume elements (RVE) [39-41]. In short, PBC ensured the portion of randomly placed CNTs that exceeded the thin film boundary would appear on the opposite edge of the film, as shown in Fig. 3. The implementation of PBC also ensured that the predetermined density or number of nanotubes was maintained. Hill *et al. [42]* explained that the characteristics of materials can be represented by a RVE, including sufficient amounts of inclusions. Odegard [39] mentioned that an RVE could represent the entire structure of the material in a statistical sense. In fact, RVE was widely employed for simulating the mechanical properties of composite materials [42,39-41]. The generated model shown in Fig. 2 utilized periodic boundary conditions. It should be mentioned that the models employed in this study was assumed to be representative of a randomly selected location of a bulk film. Therefore, its electrical and electromechanical properties would also be statistically representative of the entire system [43].

Upon generating the nanotubes in the model, junction locations were identified. A junction was defined as the location where nanotubes intersected one another. Since tunneling between neighboring nanotubes

was not considered in this research, a junction corresponded to a direct nanotube-to-nanotube intersection (*i.e.*, direct electrical contact). In addition, a soft-core model was considered such that CNT elements could penetrate one another [28,44]. In doing so, intersecting nanotubes that formed junctions remained within the same 2D plane. On the other hand, since the nanotubes employed in this work were straight, they could also be expressed as linear equations. Therefore, the locations of junctions were located by simply solving sets of linear equations, and the results were stored in a junction matrix.

In addition to being linear elements, each CNT was considered as a resistive element. Therefore, after the junction locations were identified, the equation used for calculating a nanotube's resistance (R) between junctions was defined as shown in Eq. 3 [24,45]:

$$R = R_0 + R_t + R_{jct} \tag{3}$$

where R_0 is the theoretical intrinsic resistance of a ballistic SWNT with an approximate value of 6.5 kΩ, R_t is Ohmic resistance, and R_{jct} is junction resistance. Ohmic resistance is associated with dynamic scattering of impurities (*i.e.*, optical phonons) and is defined in Eq. 4 [6]:

$$R_t = \left(\frac{h}{4e^2} \right) \frac{L_n}{l} \tag{4}$$

where h is Plank's constant, e is the electron charge, l is an electron's mean free path length (which is assumed to be 1 μm), and L_n is the conductor length (which is the length of the CNT between two junctions). Junction resistance is affected by the electrical characteristics of the junction [46]. To be specific, since a nanotube could be metallic or semiconducting depending on its chirality, the value of R_{jct} depends on junction characteristics (*i.e.*, whether it is metallic-metallic, metallic-semiconducting, or semiconducting-semiconducting) [46]. Despite these complexities, this study assumed that

junction resistance was a constant value of 98 kΩ based on the effective empirical junction resistance reported in other studies [23,24,47].

Upon calculating the resistance of CNTs between different junctions, the final step was to calculate the resistance of the entire nanotube (or equivalent resistor) network. For the purposes of this work, the top edge of the model shown in Fig. 2 is the source electrode, whereas the bottom edge is the drain. Network resistance was solved using Kirchhoff's current law and the conductance version of Ohm's law. Kirchhoff's current law states that the summation of electrical current, both input and output, at each node (or at any point) is equal to zero. The conductance version of Ohm's law expresses the conventional Ohm's law using conductance in lieu of its reciprocal or resistance. Thus, the entire resistance network can be expressed using Kirchhoff's current law in terms of conductance (Eq. 5) [6,24].

$$[G]\{v\} = \{c\} \tag{5}$$

where $[G]$ is the conductance matrix, $\{c\}$ is the equivalent current vector, and $\{v\}$ is the nodal voltage vector. The diagonal components of $[G]$ (or g_{ii}) are the summation of the conductance values connected to node i; the other elements in $[G]$ (or g_{ij}) is the negative of the conductance between nodes i and j. It should be mentioned that nodal numbers correspond to the junction numbers found earlier, and the components of $[G]$ were acquired by taking the inverse of the element resistances calculated using Eq. 3. The equivalent current source vector used in this study was determined using an assumed voltage source (*i.e.*, 10 V). The nodal voltage vector was then solved with $[G]$ and $\{c\}$. With these results, the total current was calculated using nodal voltage and the resistive nanotube elements connected to the drain (0 V). Finally, the resistance of the entire nanotube network was evaluated using the total current and the applied voltage.

Simulation of Electromechanical Response

It was shown in previous studies that CNT-based thin films subjected to mechanical deformations resulted in changes in its bulk film electrical resistance [18]. A major focus of this study was to investigate, through numerical simulations, how changes in the intrinsic piezoresistivity of individual nanotubes would affect the electromechanical behavior of the nanocomposite. Early experimental investigation by Tombler *et al.* [7] demonstrated that the conductance of a metallic SWNT decreased by more than two orders of magnitude when the tube was strained via three-point bending applied by an AFM tip. Likewise, Jang *et al.* [48] detected linear changes in resistance when both sides of an MWNT were stretched by tungsten tips. However, it remains unclear how the piezoresistivity of individual tubes affect and propagate to large-scale systems such as percolated nanotube networks.

In this study, the CNT percolation model formulated in the previous section was subjected to uniaxial tensile and compressive strains in order to quantify their electromechanical properties. For this specific implementation, tension and compression was applied in the direction of the y-axis (Fig. 2). The coordinate (0.5W, 0) was fixed, and the remainder of the film deformed accordingly and relative to this point. The fundamental assumption for updating coordinates was that the CNTs experienced perfect mechanical coupling with the polymer matrix. Therefore, applied strain (ε) deformed both the nanotubes and polymer matrix in the same way, and no stress concentrations or discontinuities existed. In addition, the Poisson's ratio of the nanocomposite was assumed to be that of typical polymers (*i.e.*, 0.34), even though an exact type of polymer matrix was neither specified nor modeled. In essence, the application of strain deformed each nanotube and altered its orientation. The coordinate of each deformed nanotube was then updated accordingly using Eqs. 6 and 7:

$$x' = x - \nu\varepsilon\left(x - \frac{W}{2}\right) \tag{6}$$

$$y' = y(1+\varepsilon) \tag{7}$$

where x and y are the initial coordinates, x' and y' are the updated coordinates, and ν is Poisson's ratio. Upon doing so, the resistance of the entire CNT network was calculated following the same procedure outlined in the previous section and before the model was subjected to a different magnitude of applied strain. It should be mentioned that only models whose CNT concentrations or densities that exceeded the percolation threshold were considered. The model's resistance was then correlated to different magnitudes of applied tensile and compressive strains for studying its electromechanical properties.

As mentioned before, an objective of this study was to quantify the effects of different CNT gage factors or strain sensitivities (S_{CNT}). In general, the definition of strain sensitivity (S) or gage factor is as follows:

$$S = \frac{\Delta R / R_0}{\varepsilon} \tag{8}$$

where R_0 is the initial unstrained resistance, ΔR is change in resistance between the strained and unstrained states, and ε is applied strain. It is known that materials such as copper and aluminum are characterized by S = 2.2 and 2.5, respectively [33]. In contrast, CNTs exhibit significantly higher gage factors as compared to conventional materials. Cao *et al. [49]* experimentally showed the intrinsic strain sensitivities of nanotubes with different electrical characteristics. For example, the strain sensitivities of small band-gap semiconducting, semiconducting, and metallic SWNTs were 1,000, 150, and 60, respectively. In this work, the numerical model assumed three different nanotube strain sensitivities (*i.e.,* S_{CNT} = 1, 60, and 150). These strain sensitivity assumptions affected the Ohmic resistance of each CNT, as was described in Eq. 4. While S_{CNT} = 60 and 150 corresponded to the metallic and semiconducting cases, respectively, S_{CNT} = 1 was treated as the

control case. When S_{CNT} = 1, the nanotube's Ohmic resistance would only depend on its length, which is directly related to the level of applied strain.

Results and Discussions

Nominal Electrical Properties

The percolation behavior of the proposed CNT-based model was evaluated using percolation probabilities. Percolation probability is defined as the probability that the CNT-based nanocomposite would possess at least one conductive path between the source and drain electrodes, thereby enabling it to conduct electrical current from one end of the film to the other. Percolation probability (P) can be calculated using Eq. 9 [50]:

$$P = \frac{n_p}{n_t} \tag{9}$$

where n_t is the total number of simulations, and n_p is the number of cases in which the model is electrically conductive. In this study, three different CNT lengths were considered (L_{CNT} = 0.14, 0.16, and 0.18 μm); it should be clarified that each simulation only considered one specific length. In addition, for each prescribed nanotube density case (*i.e.*, N nanotubes defined in the given model space), 100 simulations were conducted (n_t = 100). Nanotubes were randomly deposited in a 1×1 μm^2 area. Electrical percolation threshold (EPT) was then defined as the density of nanotubes when the CNT-based nanocomposite experienced dramatic increases in conductance and corresponded to 50% percolation probability [50].

The percolation simulation results are shown in Fig. 4. It can be observed that, as L_{CNT} increased, the number of nanotubes (or N) required for creating an electrically conductive model decreased; fewer number of CNTs were also needed to attain EPT. Specifically, when the length of nanotubes increased from 0.14 to 0.18 μm, the number of nanotubes corresponding to EPT

decreased from 290 to 180, respectively. Similarly, to reach a percolation probability of 100%, N decreased from 400 to 250. This result was expected, since the length of CNTs was equivalent to the length of the electrical conductor, and longer nanotubes had greater probabilities of intersecting another nanotube to create at least one conductive pathway that spanned from the source to the drain. These results were also consistent with other experimental and numerical investigations reported [31,50]. In addition, the percolation probability results shown in Fig. 4 were used for guiding the electrical and electromechanical simulations, as will be presented next; in these cases, only percolated thin film models that were electrically conductive were of interest.

A percolated CNT-based thin film model would be characterized by certain electrical properties, namely resistivity and conductivity. Various parameters such as nanotube length, density, aspect ratio, fabrication method, and the polymer matrix could influence the electrical properties of nanocomposites [24,51]. Despite the plethora of different parameters, this study considered only two, specifically CNT length (where L_{CNT} = 0.14, 0.16, and 0.18 μm as mentioned earlier) and nanotube density (where N = 300 to 800, in 100 increments). Fig. 5 summarizes the results after running numerous simulations (*i.e.*, 20 for each unique case) corresponding to different CNT lengths and densities. It can be seen from Fig. 5 that the resistance of the model decreased with the incorporation of longer nanotubes and with a denser nanotube network. These results were expected, because first, longer nanotubes had greater likelihood of intersecting with other nanotubes to create larger numbers of conductive pathways for a given CNT density. Similarly, by increasing the number of nanotubes within the same 2D area, more conductive pathways could also be formed, thereby increasing electrical conductivity (or decreasing resistivity). It should be noted that, as L_{CNT} and N continued to increase, the bulk film resistance began to plateau due to saturation of the number of electrical conductive pathways (Fig. 5).

Electromechanical Response

As mentioned earlier, the electromechanical properties of the thin film model were also investigated by calculating how the models' electrical properties varied with different magnitudes of applied strains. To investigate more realistic thin film models that were comparable to ones used for strain sensing applications, CNTs were deposited within a 0.5×5 μm^2 space, and periodic boundary conditions were employed again. In addition, CNTs were assigned with three different intrinsic nanotube strain sensitivities, namely S_{CNT} = 1, 60, and 150. Finally, the thin film model was subjected to uniaxial tensile-compressive cyclic strains to ±1% (in 0.025% increments), and its electrical resistance was calculated at every strain step. It should be noted that the model aimed to simulate a representative element of an actual thin film rather than the entire film subjected to electromechanical testing.

Fig. 6a shows a representative set of results corresponding to the case of a thin film model (with S_{CNT} = 150, L_{CNT} = 0.28 μm, and N = 700) subjected to cyclic loading. Fig. 6a shows the applied one-cycle load pattern to ±1%. Furthermore, the normalized change in resistance of the film (R_{norm}) was overlaid in Fig. 6a, and R_{norm} was calculated by:

$$R_{norm} = \frac{\Delta R}{R_0} \tag{13}$$

where R_0 is the initial unstrained or nominal resistance, and ΔR is change in resistance between the strained and unstrained states. The fact that the model's electrical resistance changed in response to strain confirmed the electromechanical properties observed by many other research groups. Fig. 6b plots the normalized change in resistance as a function of applied strains. From Fig. 6b, one could conclude that the normalized change in resistance varied linearly when the film was strained in both tension and compression. A linear least-squares regression line was also fit to the raw data shown in Fig. 6b to demonstrate the model's strong linearity. It should be noted that many other CNT-based thin film models also exhibited such linearity. Similar

electromechanical properties were also observed in numerous other experimental studies [15,18,52,53].

Despite the similarities, the model employed in this study only investigated a small representative element of what was typically tested in the aforementioned experimental studies and not the entire film. In addition, the conditions of the model were specific to films under perfectly uniform, uniaxial, tensile-compressive cyclic loading. In experiments, such ideal conditions may not exist, so comparison of numerical and experimental results needs to be performed with caution. This is particularly true for freestanding films subjected to tensile tests where non-uniform stress distributions could occur near its boundaries. However, such effects can be negligible if the specimen tested is large enough such that the majority of the film is subjected to uniaxial loading. In this case, the model results can serve as a good comparison.

Nevertheless, the results from a few models that incorporated higher nanotube strain sensitivities (*i.e.*, S_{CNT} = 60 and 150) showed nonlinear piezoresistivity at relatively higher strains (ε > 2,500 $\mu\varepsilon$) (see Fig. 7). This result could be explained by the model's assumption in which the thin film resistance depended on the CNTs' intrinsic gage factor, as well as their length and orientation, at different levels of applied strains. Despite this, a linear least-squares regression line could be fitted to the raw data shown in Fig. 7b (and similarly in Fig. 6b), and the slope of the best-fit line was also the strain sensitivity of the modeled film. In particular, it can be seen from Fig. 7b that the model's normalized change in resistance deviated from the linear response shown in Fig. 6b.

Thin Film Strain Sensitivity

Upon executing all the different numerical simulations that employed different numbers of nanotubes, lengths, and intrinsic strain sensitivities, the

results are summarized in Fig. 8. The lowest nanotube concentration (*i.e.*, N = 330) for the thin film strain sensitivity simulation was chosen based on percolation probability results in which percolation probability was ~50%. Here, each data point corresponds to the average strain sensitivity determined from 20 simulations; the only exception was those cases in which the films were near the percolation threshold, and 40 simulations were conducted. From Fig. 8, it can be observed that, when S_{CNT} = 1, the strain sensitivity of the bulk film was very low and decreased marginally as CNT density or N was increased. On the other hand, clear trends could be identified for the other two cases when S_{CNT} = 60 or 150. As N was increased from 330 to 800, bulk film strain sensitivity decreased. It should be noted that with higher CNT gage factors (*i.e.*, S_{CNT} = 150), bulk film strain sensitivity was also higher as compared to films with the same CNT concentration but with a lower intrinsic CNT gage factor. When CNT strain sensitivity was 1, the film's resistance response only depended on changes in nanotube lengths. On the other hand, with larger S_{CNT}, resistance changes were amplified to result in high bulk film strain sensitivities, which were consistent with other experimental and numerical studies [20,54,31]. However, regardless of S_{CNT}, the same trends existed in which strain sensitivity decreased with increasing CNT density.

This study also investigated how bulk film strain sensitivities varied near percolation and when even longer nanotubes were incorporated. Similar to previous cases, CNTs were deposited within a 0.5×5 μm^2 space. On the other hand, the length of nanotubes was varied as follows, where L_{CNT} = 0.213 to 0.53 μm for N = 500, and L_{CNT} = 0.195 to 0.4 μm for N = 600. Numerical simulations of films subjected to tensile-compressive loading were conducted, and the strain sensitivities corresponding to the different cases were calculated as before. It should be noted that the shortest CNT length was also decided based on percolation probability results; specifically, the shortest nanotube length corresponded to the case that yielded only 50%

percolation probability. Here, a total of 20 simulations were performed for each CNT density case, except 30 simulations were conducted near the percolation threshold.

The strain sensitivity results are shown in Fig. 9. Similar to the results shown Fig. 8, strain sensitivity decreased as nanotube length increased. The major difference observed in this case, however, was strain sensitivity near percolation. Here, the trend near percolation was inconsistent, where it appeared that strain sensitivity peaked not when percolation probability was 50% but at higher values (*i.e.*, still close to percolation). It should be noted that inconsistent strain sensitivity near percolation threshold was clearer for strain sensitivity results as a function of nanotube lengths (Fig. 9) than that of nanotube concentration (Fig. 8). A possible explanation could be due to the inherent randomness of the model, where the electrical and electromechanical properties were affected by how CNTs were distributed in the film. As a result, models close to percolation (*i.e.*, with low CNT densities) would be sensitive to special cases that could occur. Amini *et al.* [31] demonstrated through numerical modeling that, when the concentration of MWNTs was near the percolation threshold, the electrical properties deviated more than that of higher MWNTs concentrations. One could infer that higher strain sensitivities could be acquired near the percolation threshold, but the repeatability would be lower as compared to relatively higher nanotube concentrations [31].

Conclusions

In this study, 2D percolation-based computational models were developed to investigate the electrical and electromechanical properties of CNT-based nanocomposites. First, straight nanotubes were randomly distributed in a 2D representative area of a thin film. Then, CNT junction locations were found

by solving sets of linear equations that defined the position and orientation of each nanotube. With the nanotube resistor network defined and the location of junctions known, the electrical resistance of the entire model was then calculated using Kirchhoff's current law and the conductance version of Ohm's law. The numerical model was then subjected to uniaxial tensile-compressive cyclic strains in an effort to study the electromechanical responses of the nanocomposite system. In particular, the objective was to characterize how the electrical properties of the thin film model would vary depending on different CNT lengths, densities, and intrinsic CNT piezoresistivity considered.

First, the numerical model was used for investigating percolation properties. It was found that the electrical percolation threshold decreased with the incorporation of longer nanotubes, since longer CNTs possessed a greater probability of intersecting with another longer tube in its vicinity. Second, the unstrained or nominal electrical resistance of nanocomposites with different CNT lengths and densities were determined. The results showed that electrical resistance decreased with the incorporation of longer nanotubes and at higher nanotube concentrations, both of which were expected. Finally, the thin film's electromechanical or strain-sensitive properties were also studied. It was found that the bulk film's resistance increased with increasingly applied tensile strains, and the opposite was also true (*i.e.*, resistance decreased with greater compression). The results also showed that strain sensitivity decreased with increasing CNT lengths, regardless of their intrinsic gage factor used. However, this trend was not true when the film was close to the percolation threshold. In addition, non-linear response at high strains was also observed when higher values of CNT gage factors were considered.

Acknowledgements

The authors thank the U.S. National Science Foundation (NSF), under grant number CMMI-CAREER 1253564, for the support of this research.

References

[1] Coleman JN, Khan U, Gun'ko YK (2006) Mechanical reinforcement of polymers using carbon nanotubes. Adv Mater 18:689-706.

[2] Tsukagoshi K, Yoneya N, Uryu S, Aoyagi Y, Kanda A, Ootuka Y, Alphenaar BW (2002) Carbon nanotube devices for nanoelectronics. Physica B: Condensed Matter 323:107-114.

[3] Baughman RH, Zakhidov AA, de Heer WA (2002) Carbon nanotubes-the route toward applications. Science 297:787-792.

[4] De Volder MFL, Tawfick SH, Baughman RH, Hart AJ (2013) Carbon nanotubes: present and future commercial applications. Science 339:535-539.

[5] Javey A, Guo J, Wang Q, Lundstrom M, Dai H (2003) Ballistic carbon nanotube field-effect transistors. Nature 424:654-657.

[6] Bandaru PR (2007) Electrical properties and applications of carbon nanotube structures. J Nanosci Nanotechnol 7:1-29.

[7] Tombler TW, Zhou C, Alexseyev L, Kong J, Dai H, Liu L, Jayanthi CS, Tang M, Wu S-Y (2000) Reversible electromechanical characteristics of carbon nanotubes under local-probe manipulation. Nature 405:769-772.

[8] Li QW, Li Y, Zhang XF, Chikkannanavar SB, Zhao YH, Dangelewicz AM, Zheng LX, Doorn SK, Jia QX, Peterson DE, Arendt PN, Zhu YT (2007) Structure-dependent electrical properties of carbon nanotube fibers. Adv Mater 19:3358-3363.

[9] Vaisman L, Wagner HD, Marom G (2006) The role of surfactants in dispersion of carbon nanotubes. Adv Colloid Interface Sci 128–130:37-46.

[10] Loh KJ-H (2008) Development of multifunctional carbon nanotube nanocomposite sensors for structural health monitoring. PhD Dissertation, University of Michigan

[11] Breuer O, Sundararaj U (2004) Big returns from small fibers: A review of polymer/carbon nanotube composites. Polym Compos 25:630-645.

[12] Blanco J, García EJ, Guzmán de Villoria R, Wardle BL (2009) Limiting mechanisms of Mode I interlaminar toughening of composites reinforced with aligned carbon nanotubes. J Compos Mater 43:825-841.

[13] Gojny FH, Wichmann MHG, Köpke U, Fiedler B, Schulte K (2004) Carbon nanotube-reinforced epoxy-composites: enhanced stiffness and fracture toughness at low nanotube content. Compos Sci Technol 64:2363-2371.

[14] Qian D, Dickey EC, Andrews R, Rantell T (2000) Load transfer and deformation mechanisms in carbon nanotube-polystyrene composites. Appl Phys Lett 76:2868-2870.

[15] Dharap P, Li Z, Nagarajaiah S, Barrera EV (2004) Nanotube film based on single-wall carbon nanotubes for strain sensing. Nanotechnol 15:379.

[16] Li Z, Dharap P, Nagarajaiah S, Barrera EV, Kim JD (2004) Carbon nanotube film sensors. Adv Mater 16:640-643.

[17] Kang I, Schulz MJ, Kim JH, Shanov V, Shi D (2006) A carbon nanotube strain sensor for structural health monitoring. Smart Mater Struct 15:737.

[18] Loh KJ, Kim J, Lynch JP, Kam NWS, Kotov NA (2007) Multifunctional layer-by-layer carbon nanotube–polyelectrolyte thin films for strain and corrosion sensing. Smart Mater Struct 16:429.

[19] Loh KJ, Lynch JP, Shim BS, Kotov NA (2008) Tailoring piezoresistive sensitivity of multilayer carbon nanotube composite strain sensors. JIMSS 19:747-764.

[20] Pham GT, Park YB, Liang Z, Zhang C, Wang B (2008) Processing and modeling of conductive thermoplastic/carbon nanotube films for strain sensing. Composites Part B 39:209-216.

[21] Park M, Kim H, Youngblood JP (2008) Strain-dependent electrical resistance of multi-walled carbon nanotube/polymer composite films. Nanotechnol 19:055705.

[22] Loyola B, La Saponara V, Loh K (2010) In situ strain monitoring of fiber-reinforced polymers using embedded piezoresistive nanocomposites. JMatS 45:6786-6798.

[23] Kumar S, Murthy JY, Alam MA (2005) Percolating conduction in finite nanotube networks. Phys Rev Lett 95:066802.

[24] Behnam A, Ural A (2007) Computational study of geometry-dependent resistivity scaling in single-walled carbon nanotube films. Phys Rev B 75:125432.

[25] Li C, Thostenson ET, Chou T-W (2008) Effect of nanotube waviness on the electrical conductivity of carbon nanotube-based composites. Compos Sci Technol 68:1445-1452.

[26] Du F, Fischer JE, Winey KI (2005) Effect of nanotube alignment on percolation conductivity in carbon nanotube/polymer composites. Phys Rev B 72:121404.

[27] Bao WS, Meguid SA, Zhu ZH, Meguid MJ (2011) Modeling electrical conductivities of nanocomposites with aligned carbon nanotubes. Nanotechnol 22:485704.

[28] Hu N, Karube Y, Yan C, Masuda Z, Fukunaga H (2008) Tunneling effect in a polymer/carbon nanotube nanocomposite strain sensor. Acta Mater 56:2929-2936.

[29] Hu N, Karube Y, Arai M, Watanabe T, Yan C, Li Y, Liu Y, Fukunaga H (2010) Investigation on sensitivity of a polymer/carbon nanotube composite strain sensor. Carbon 48:680-687.

[30] Rahman R, Servati P (2012) Effects of inter-tube distance and alignment on tunnelling resistance and strain sensitivity of nanotube/polymer composite films. Nanotechnol 23:055703.

[31] Amini A, Bahreyni B (2012) Behavioral model for electrical response and strain sensitivity of nanotube-based nanocomposite materials. J Vac Sci Technol B 30.

[32] Wang Z, Ye X (2013) A numerical investigation on piezoresistive behaviour of carbon nanotube/polymer composites: mechanism and optimizing principle. Nanotechnol 24:265704.

[33] Stampfer C, Jungen A, Linderman R, Obergfell D, Roth S, Hierold C (2006) Nano-electromechanical displacement sensing based on single-walled carbon nanotubes. Nano Lett 6:1449-1453.

[34] Cullinan MA, Culpepper ML (2010) Carbon nanotubes as piezoresistive microelectromechanical sensors: Theory and experiment. Phys Rev B 82:115428.

[35] Broadbent SR, Hammersley JM (1957) Percolation processes. MPCPS 53:629-641.

[36] Hammersley JM (1957) Percolation Processes: Lower Bounds for the Critical Probability. The Annals of Mathematical Statistics 28:790-795.

[37] Kirkpatrick S (1973) Percolation and Conduction. Rev Mod Phys 45:574-588.

[38] Lee BM, Loh KJ, Burton A, Loyola BR (2014) Modeling the electromechanical and strain response of carbon nanotube-based nanocomposites. Paper presented at the SPIE, San Diego, CA,

[39] Odegard G (2009) Multiscale modeling of nanocomposite materials. In: Farahmand B (ed) Virtual Testing and Predictive Modeling. Springer US, pp 221-245. doi:10.1007/978-0-387-95924-5_8

[40] Harper LT, Qian C, Turner TA, Li S, Warrior NA (2012) Representative volume elements for discontinuous carbon fibre composites – Part 1: Boundary conditions. Compos Sci Technol 72:225-234.

[41] Kanit T, Forest S, Galliet I, Mounoury V, Jeulin D (2003) Determination of the size of the representative volume element for random composites: statistical and numerical approach. IJSS 40:3647-3679.

[42] Hill R (1963) Elastic properties of reinforced solids: Some theoretical principles. J Mech Phys Solids 11:357-372.

[43] Alamusi, Hu N, Fukunaga H, Atobe S, Liu Y, Li J (2011) Piezoresistive Strain Sensors Made from Carbon Nanotubes Based Polymer Nanocomposites. Sensors 11:10691-10723.

[44] Berhan L, Sastry AM (2007) Modeling percolation in high-aspect-ratio fiber systems. I. Soft-core versus hard-core models. PhRvE 75:041120.

[45] McEuen PL, Park JY (2004) Electron transport in single-walled carbon nanotubes. MRS Bull 29:272-275.

[46] Fuhrer MS, Nygård J, Shih L, Forero M, Yoon Y-G, Mazzoni MSC, Choi HJ, Ihm J, Louie SG, Zettl A, McEuen PL (2000) Crossed nanotube junctions. Science 288:494-497.

[47] Nirmalraj PN, Lyons PE, De S, Coleman JN, Boland JJ (2009) Electrical connectivity in single-walled carbon nanotube networks. Nano Lett 9:3890-3895.

[48] Jang H-S, Lee Y-H, Na H-J, Nahm SH (2008) Variation in electrical resistance versus strain of an individual multiwalled carbon nanotube. JAP 104.

[49] Cao J, Wang Q, Dai H (2003) Electromechanical properties of metallic, quasimetallic, and semiconducting carbon nanotubes under stretching. Phys Rev Lett 90:157601.

[50] Zeng X, Xu X, Shenai PM, Kovalev E, Baudot C, Mathews N, Zhao Y (2011) Characteristics of the electrical percolation in carbon nanotubes/polymer nanocomposites. J Phys Chem C 115:21685-21690.

[51] Bauhofer W, Kovacs JZ (2009) A review and analysis of electrical percolation in carbon nanotube polymer composites. Compos Sci Technol 69:1486-1498.

[52] Lee D, Hong HP, Lee CJ, Park CW, Min NK (2011) Microfabrication and characterization of spray-coated single-wall carbon nanotube film strain gauges. Nanotechnol 22:455301.

[53] Li X, Levy C, Elaadil L (2008) Multiwalled carbon nanotube film for strain sensing. Nanotechnol 19:045501.

[54] Jang J, Cha S, Choi Y, Amaratunga GA, Kang D, Hasko D, Jung J, Kim J (2005) Nanoelectromechanical switches with vertically aligned carbon nanotubes. Appl Phys Lett 87:163114.

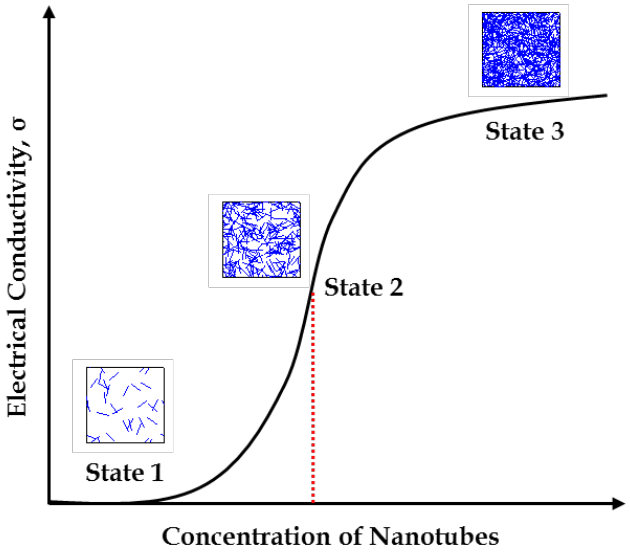

Fig. 1 The electrical conductivity of CNT-based nanocomposites follows percolation theory and can be classified by three different states. State 1 is an electrically insulating state where very few nanotubes are distributed nor connected to one another. State 2 experiences dramatic increases in conductivity as a result of the creation of at least one or a few electrically conductive pathways between opposite electrodes. State 3 consists of a dense network of electrically conductive paths

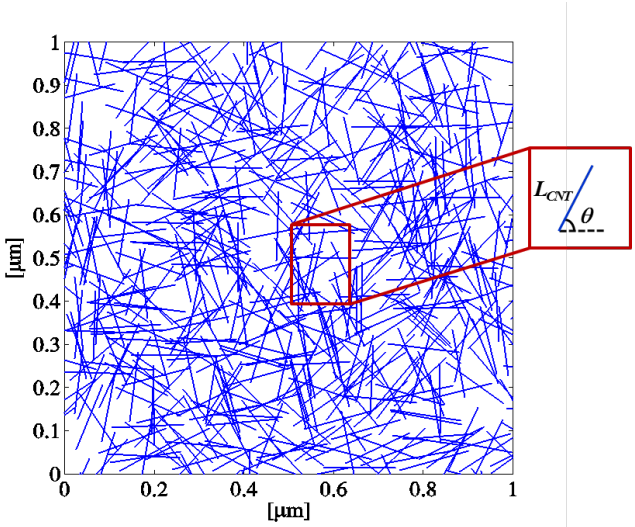

Fig. 2 Nanotubes were randomly distributed in the representative 2D unit area model (1×1 μm^2) with a prescribed nanotube length (L_{CNT} = 0.16 μm), nanotube concentration (N = 600), and the use of periodic boundary conditions

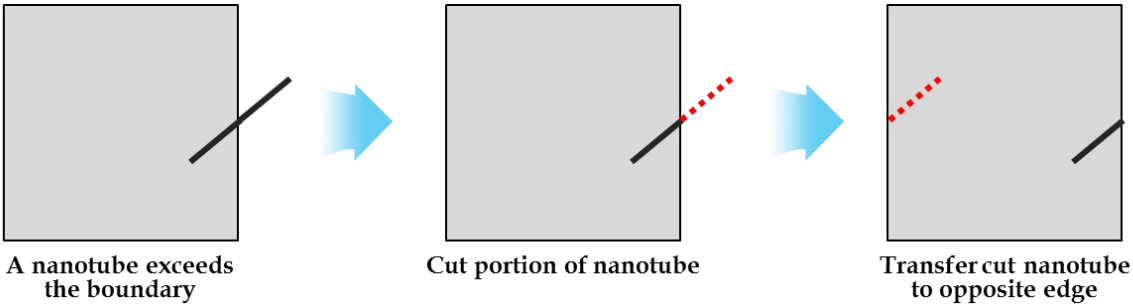

Fig. 3 Periodic boundary conditions were implemented in this study by cutting the nanotubes that exceeded the model boundary and then transferring them to the opposite edge

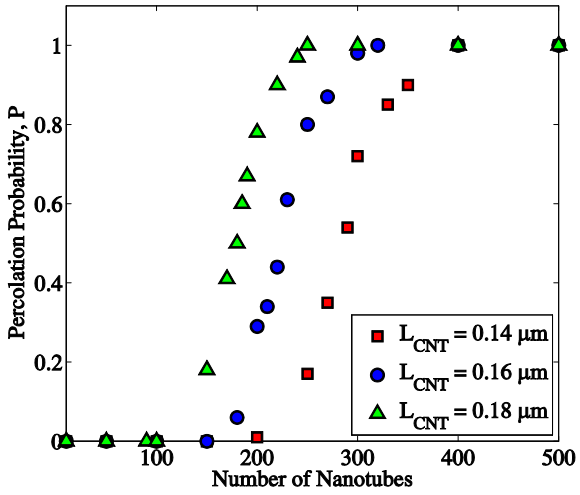

Fig. 4 The percolation characteristics of 1×1 μm^2 CNT-based nanocomposite models were evaluated as a function of nanotube concentration. Three different nanotube lengths (L_{CNT} = 0.14, 0.16, and 0.18 μm) were considered

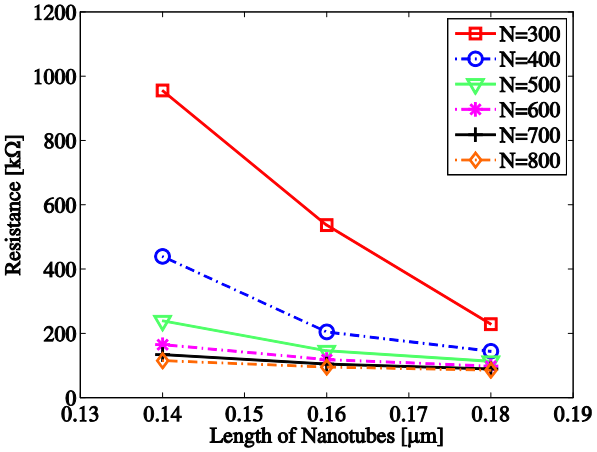

Fig. 5 The nominal unstrained resistances of 1×1 μm^2 CNT-based nanocomposite models were evaluated with different nanotube lengths (L_{CNT} = 0.14, 0.16, and 0.18 μm) and concentrations (N)

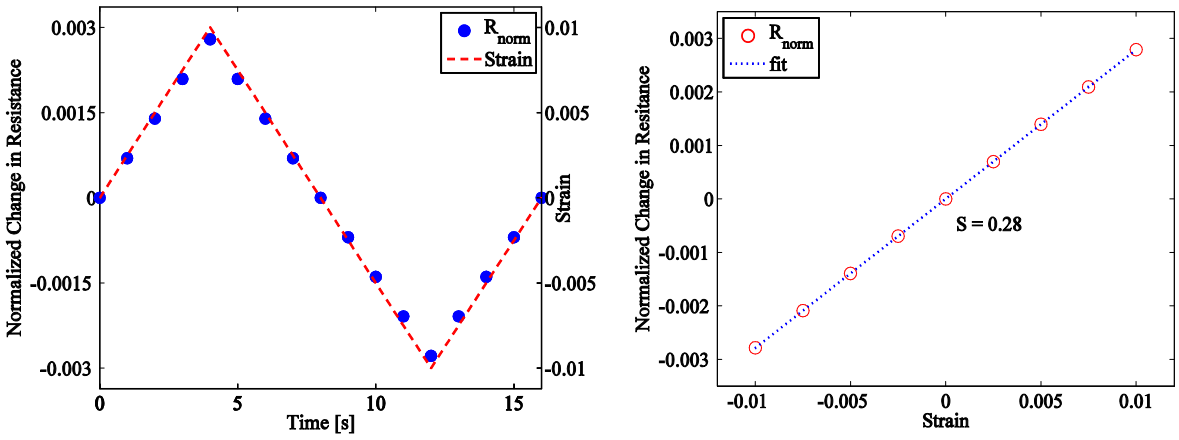

Fig. 6 (a) The CNT-based nanocomposite model (0.5×5 μm^2) exhibited linear piezoresistivity when subjected to a one-cycle tensile-compressive strain pattern to ±1%. The model assumed that S_{CNT} =150, L_{CNT} = 0.28 μm, and N = 700. (b) The corresponding film's normalized change in resistance was plotted as a function of strain, and the strain sensitivity of this model was 0.28

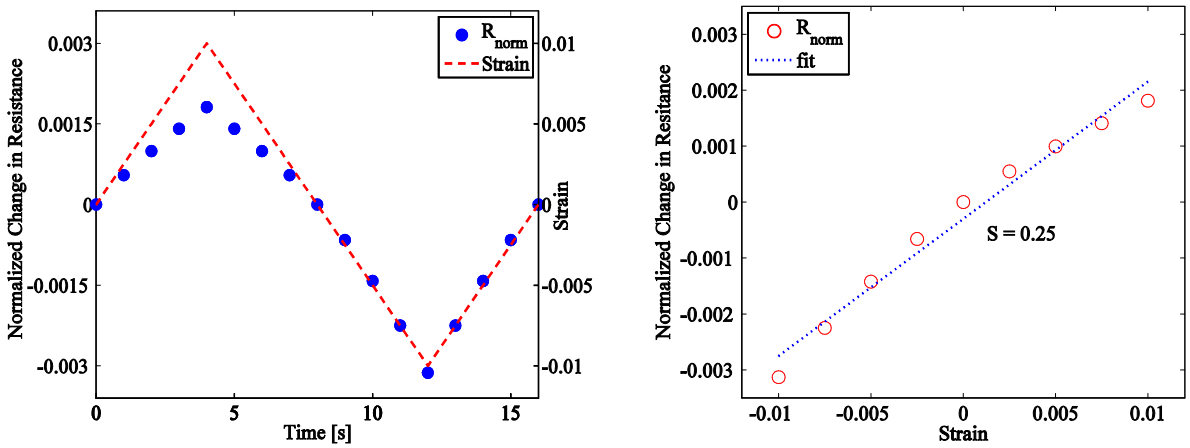

(a) (b)

Fig. 7 (a) Certain thin film models showed non-linear piezoresistivity. This model assumed that S_{CNT} = 150, L_{CNT} = 0.28 μm, and N = 700. (b) The corresponding film's normalized change in resistance was plotted as a function of strain, and the bulk film strain sensitivity was ~0.25

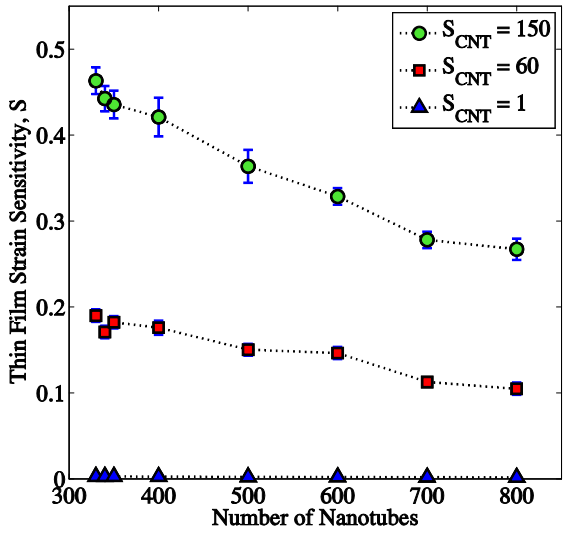

Fig. 8 The strain sensitivities of 0.5×5 μm^2 CNT-based thin film models with three different intrinsic CNT gage factors (S_{CNT} = 1, 60, and 150) and different nanotube concentrations were determined. The average strain sensitivities and corresponding error bars (*i.e.*, standard error of the mean) are shown

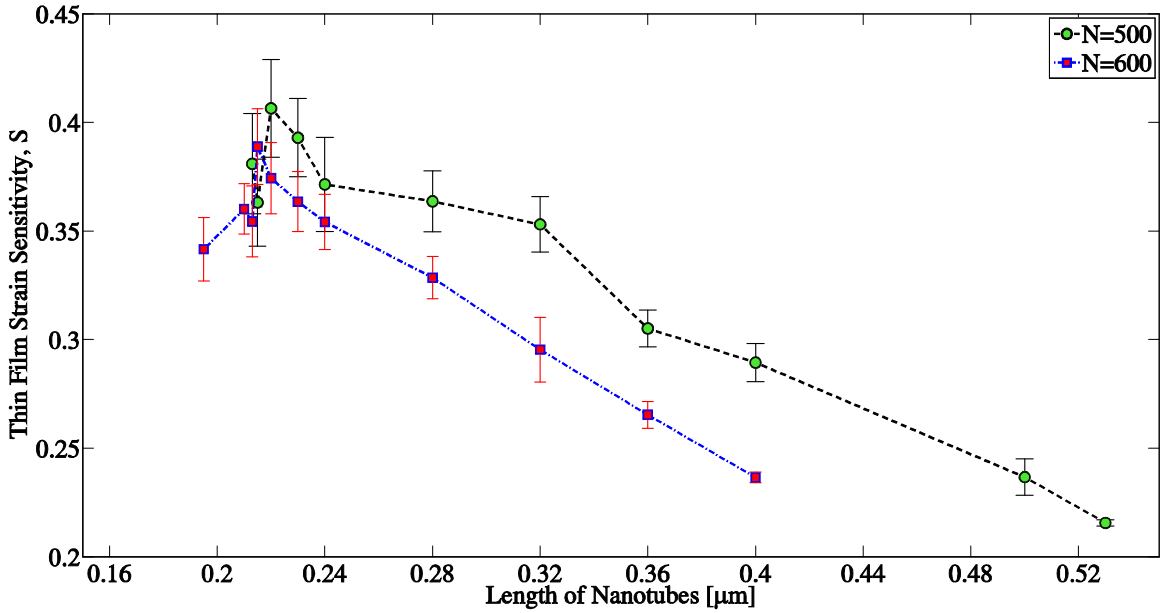

Fig. 9 The average bulk film strain sensitivities were estimated as a function of nanotube length. Two different nanotube concentration cases (*i.e.*, N = 500 and 600) were considered, and their corresponding error bars (*i.e.*, standard error of the mean) are also plotted